

# Increasing Si photodetector photosensitivity in near-infrared region and manifestation of optical amplification by dressed photons

H. Tanaka · T. Kawazoe · M. Ohtsu

Received: 22 March 2012 / Published online: 24 May 2012

© The Author(s) 2012. This article is published with open access at Springerlink.com

**Abstract** We fabricated a novel photodetector by subjecting a Si crystal having a p–n homojunction to phonon-assisted annealing. The photosensitivity of this device for incident light having a wavelength of 1.16  $\mu\text{m}$  or greater was about three times higher than that of a reference Si-PIN photodiode. The photosensitivity was increased for incident light with a wavelength of 1.32  $\mu\text{m}$  by applying a forward current. When the forward current density was 9  $\text{A}/\text{cm}^2$ , a photosensitivity of 0.10  $\text{A}/\text{W}$  was achieved. This value is at least 4000 times higher than the zero-bias photosensitivity. This remarkable increase was due to the manifestation of optical amplification cause by the forward current injection. For a forward current density of 9  $\text{A}/\text{cm}^2$ , the small-signal gain coefficient of the optical amplification was  $2.2 \times 10^{-2}$ , and the saturation power was  $7.1 \times 10^2 \text{ mW}$ .

## 1 Introduction

Silicon (Si) is an abundant material in the Earth's crust and has low toxicity, and it is widely used as a material for many electronic and optical devices. For example, Si photodetectors (Si-PDs) are widely used photoelectric conversion

devices; however, their photosensitivity limit at the long-wavelength side is limited by the bandgap energy,  $E_g$ , of Si ( $= 1.12 \text{ eV}$ ) [1], and the photosensitivity drops rapidly at wavelengths above 1.11  $\mu\text{m}$ . Because of this, materials such as Ge [2], InGaAsP [3], and InGaAs [4] that have a smaller  $E_g$  than Si have been used in optical fiber communications. However, Ge photodetectors have a large dark current, and cooling is required in many cases. In addition, InGaAs photodetectors suffer from problems such as the use of highly toxic metal-organic materials in their fabrication, high cost, and so forth, and recently, depletion of resources, such as In, has also been a problem. If the photosensitivity limit of Si-PDs could be extended past the 1.11  $\mu\text{m}$  wavelength into the near-infrared region at 1.3  $\mu\text{m}$  and above, these problems could be overcome. An additional benefit of Si-PDs is their high compatibility with electronic devices. For this reason, photoelectric conversion devices exploiting effects such as mid-bandgap absorption [5–7], surface-state absorption [8, 9], internal photoemission absorption [10, 11], and two-photon absorption [12, 13] in Si have been reported in the literature. However, in the case of mid-bandgap absorption, for example, the photosensitivity at a wavelength of 1.3  $\mu\text{m}$  is limited to only 50  $\text{mA}/\text{W}$  [5].

In this research, we realized a novel Si-PD with increased photosensitivity. We applied the same fabrication method and light emission principle of a silicon light emitting diode (Si-LED) based on a phonon-assisted process that we previously proposed [14, 15]. Specifically, while radiating light, Joule-heat annealing was performed to control the spatial distribution of the impurity (boron) concentration in a Si crystal in a self-organized manner, to efficiently generate dressed photons. The photocurrent of the novel Si-PD fabricated by this method was varied by a stimulated emission process driven by the incident light. Because this stimulated emission process caused optical amplification, the photosen-

H. Tanaka · T. Kawazoe (✉) · M. Ohtsu  
Department of Electrical Engineering and Information Systems,  
Graduate School of Engineering, The University of Tokyo,  
2-11-16 Yayoi, Bunkyo-ku, Tokyo 113-8656, Japan  
e-mail: [kawazoe@ee.t.u-tokyo.ac.jp](mailto:kawazoe@ee.t.u-tokyo.ac.jp)  
Fax: +81-3-58411140

T. Kawazoe · M. Ohtsu  
Nanophotonics Research Center, Graduate School of  
Engineering, The University of Tokyo, 2-11-16 Yayoi,  
Bunkyo-ku, Tokyo 113-8656, Japan

sitivity of this Si-PD was remarkably increased. The operating principle of the Si-PD is described in Sect. 2, the fabrication method is described in Sect. 3, device characterization and evaluation results are presented in Sect. 4, and the paper concludes with Sect. 5.

## 2 Operating principle

The operating principle of the Si-PD fabricated in this research is based on a phonon-assisted process caused by dressed photons [16–20]. A dressed photon is a quasi-particle representing a coupled state between a photon and an electron at the nanoscale. The phonon-assisted process originates in the property of a dressed photon to couple with a phonon. By using this property, it is possible to create an electron–hole pair via a two-step excitation even with photons having an energy smaller than the bandgap energy,  $E_g$ , of the semiconductor. Therefore, the Si-PD can exhibit photosensitivity even for infrared light with a photon energy smaller than  $E_g$ . This principle has already been applied to photochemical vapor deposition [16], photovoltaic devices [17], photolithography [18], subnanometer polishing of a glass surface [19], optical frequency up-conversion [20], and other applications.

Electrons in the Si-PD experience a two-step excitation via processes (1) and (2) described below. (These processes (1) and (2), as well as processes (1′) and (2′) described later, are the same as those in the Si-LED previously proposed by the authors; for details, refer to Ref. [14] and Fig. 1 therein.)

- (1) First step: The electron is excited from the initial ground state  $|E_g; el\rangle \otimes |E_{\text{exthermal}}; \text{phonon}\rangle$  to intermediate state  $|E_g; el\rangle \otimes |E_{\text{ex}}; \text{phonon}\rangle$ . Here,  $|E_g; el\rangle$  represents the ground state (valence band) of the electron, and  $|E_{\text{exthermal}}; \text{phonon}\rangle$  and  $|E_{\text{ex}}; \text{phonon}\rangle$  respectively represent the excited state of the phonon determined by the crystal lattice temperature and the excited state of the phonon determined by the dressed photon energy. The symbol  $\otimes$  represents the direct product of the ket vectors. Because this is an electric-dipole–forbidden transition, a dressed photon is essential for the excitation.
- (2) Second step: The electron is excited from the intermediate state  $|E_g; el\rangle \otimes |E_{\text{ex}}; \text{phonon}\rangle$  to the final state  $|E_{\text{ex}}; el\rangle \otimes |E_{\text{ex}}; \text{phonon}\rangle$ . Here,  $|E_{\text{ex}}; el\rangle$  represents the excited state (conduction band) of the electron, and  $|E_{\text{ex}}; \text{phonon}\rangle$  represents the excited state of the phonon. Because this is an electric-dipole–allowed transition, the electron is excited not only by the dressed photon but also by propagating light. After this excitation, the phonon in the excited state relaxes to a thermal equilibrium state having an occupation probability determined by the crystal lattice temperature,

which completes excitation to the electron excited state  $|E_{\text{ex}}; el\rangle \otimes |E_{\text{exthermal}}; \text{phonon}\rangle$ .

Because a phonon is involved in the above excitation of the electron, this excitation process is known as a phonon-assisted process [16–20]. When light having a photon energy smaller than  $E_g$  is incident on the Si-PD, electrons are excited by the two-step excitation described above, generating a photocurrent. Photosensitivity to this incident light is manifested by means of the above process.

Note that applying a forward current to the Si-PD causes the two-step stimulated emission described by processes (1′) and (2′) below [17].

- (1′) First step: When a forward current is applied, an electron is injected from the external circuit to the conduction band, and therefore, the state  $|E_{\text{ex}}; el\rangle \otimes |E_{\text{exthermal}}; \text{phonon}\rangle$  is the initial state. During this time, driven by a dressed photon generated in the p–n junction of the Si-PD by the incident light, the electron transitions from the initial state  $|E_{\text{ex}}; el\rangle \otimes |E_{\text{exthermal}}; \text{phonon}\rangle$  to an intermediate state  $|E_g; el\rangle \otimes |E_{\text{ex}}; \text{phonon}\rangle$ , creating a dressed photon and propagating light via stimulated emission. Because Si is an indirect-transition-type semiconductor, there are almost no transitions caused by spontaneous emission.
- (2′) Second step: The electron transitions from the intermediate state  $|E_g; el\rangle \otimes |E_{\text{ex}}; \text{phonon}\rangle$  to a final state  $|E_{\text{ex}}; el\rangle \otimes |E_{\text{ex}}; \text{phonon}\rangle$ , causing stimulated emission. Because this is an electric-dipole–forbidden transition, only a dressed photon is generated. After this transition, the phonon in the excited state relaxes to a thermal equilibrium state determined by the crystal lattice temperature, which completes the transition to the electron ground state  $|E_g; el\rangle \otimes |E_{\text{exthermal}}; \text{phonon}\rangle$ .

Here, if the electron number densities occupying the initial state  $|E_{\text{ex}}; el\rangle \otimes |E_{\text{exthermal}}; \text{phonon}\rangle$  and the intermediate state  $|E_g; el\rangle \otimes |E_{\text{ex}}; \text{phonon}\rangle$ ,  $n_{\text{ex}}$  and  $n_{\text{inter}}$ , satisfy the Bernard–Duraffourg inversion condition ( $n_{\text{ex}} > n_{\text{inter}}$ ) [21], the number of photons created by stimulated emission exceeds the number of photons annihilated by absorption. In other words, optical amplification occurs. Because the amplified light brings about processes (1′) and (2′) again via dressed photons, the photosensitivity of the Si-PD in the case where a forward current is applied far exceeds the photosensitivity based on only processes (1) and (2).

## 3 Fabrication method

To realize the optical amplification described in Sect. 2, it is essential to efficiently generate dressed photons in the p–n junction of the Si-PD. To do so, we adopted a Si-LED fabrication method that we previously proposed [14]. In this

method, Joule-heat annealing was performed while radiating 1.32  $\mu\text{m}$ -wavelength light.

First, an n-type silicon substrate with an electrical resistivity of 10  $\Omega\text{ cm}$  and a thickness of 625  $\mu\text{m}$ , doped with arsenic (As), was used as the Si-PD material. This substrate was doped with boron (B) via ion implantation to form a p-layer. For the B doping, the implantation energy was 700 keV, and the ion dose density was  $5 \times 10^{13}\text{ cm}^{-2}$ . After forming a p–n homojunction in this way, an indium tin oxide (ITO) film with a thickness of 150 nm was deposited at the p-layer side, a chromium film and an aluminum film with thicknesses of 5 nm and 80 nm were deposited at the n-substrate side, all by RF sputtering, and these were used as positive and negative electrodes. Then, the silicon substrate with these electrodes attached was diced with a dicer to form a single Si-PD. The area was about 2  $\text{mm}^2$ .

Next, annealing was performed by applying a forward current to the Si-PD to generate Joule heating, causing the B to diffuse and changing the spatial distribution of the B concentration. During this time, the device was irradiated, from the ITO electrode side, with laser light having a photon energy smaller than  $E_g$  of Si ( $E_g$  of 0.9 eV, corresponding to a wavelength of 1.32  $\mu\text{m}$ , and optical power of 120 mW). This induced the phonon-assisted process, and the B diffusion due to the annealing was controlled. As a result, a B concentration with a spatial distribution suitable for efficiently generating dressed photons was formed in a self-organized manner.

The above method is the same as the method of fabricating Si-LEDs previously reported by the authors [14, 15]. Here, however, in order to make use of the stimulated emission process described in Sect. 2 for the Si-PD to be fabricated, it is necessary to make the probability of generating stimulated emission larger than the probability of generating spontaneous emission. To do so, the forward current density for annealing was kept smaller than that in Ref. [14], namely, 1.3  $\text{A}/\text{cm}^2$ . Determining the number of injected electrons per unit time and per unit area on this basis gives a value of  $8.1 \times 10^{18}\text{ s}^{-1}\text{ cm}^{-2}$ , which corresponds to the probability of generating spontaneous emission. On the other hand, the generation probability of stimulated emission corresponds to the number of photons per unit time and per unit area, which is  $3.9 \times 10^{19}\text{ s}^{-1}\text{ cm}^{-2}$  in the case of the laser power mentioned above (120 mW). Comparing this with the number of injected electrons confirms that the probability of generating stimulated emission is sufficiently large.

When performing Joule-heat annealing under laser irradiation in practice, the surface temperature of the Si-PD, measured by thermography, showed a temporal variation similar to Fig. 2(c) in Ref. [14]. Specifically, immediately after applying the forward current, the surface temperature rose to 40.7  $^{\circ}\text{C}$ , then dropped due to the generation of stimulated emission and dissipation of its associated Joule energy,

and reached an almost stable temperature (38.6  $^{\circ}\text{C}$ ) after about 10 minutes, at which point the annealing was completed.

## 4 Device characterization

In this section we present the results of evaluating the spectral sensitivity characteristics, the voltage–current characteristics, and the optical amplification characteristics of the fabricated device.

### 4.1 Spectral sensitivity characteristics

First, we measured the spectral sensitivity characteristics when a forward current was not applied to the device. Photoelectric conversion in this case is based on the two-step excitation described by processes (1) and (2) in Sect. 2. As the light source, we used a xenon lamp, for wavelength selection we used a monochromator, and for photocurrent detection we used a lock-in amplifier. The optical power at each wavelength was measured with an InGaAs photodiode (Hamamatsu Photonics, G8370). The measurement wavelength range was 1.00–1.20  $\mu\text{m}$ . The spectral sensitivity characteristics measured in the infrared region are shown by curves A to C in Fig. 1. Curve A shows the values obtained with a Si-PD fabricated by annealing using the phonon-assisted process described in Sect. 3. For comparison, curve B shows values obtained with a Si-PD fabricated without annealing. Curve C shows the values obtained with a Si-PIN photodiode (Hamamatsu Photonics, S3590) used as a reference. Comparing curves A and C, the photosensitivities of both of them were reduced in the wavelength region longer than a cutoff wavelength  $\lambda_c = 1.11\text{ }\mu\text{m}$  determined by  $E_g$  of Si, although in curve A the reduction was more gentle, and at wavelengths above 1.16  $\mu\text{m}$ , the photosensitivity was about three times higher than that of curve C. In addition, the photosensitivity values for curve A were larger than the values for curve B. This was due to the spatial distribution of the B concentration being controlled in a self-organized manner so that dressed photons are efficiently generated by annealing using the phonon-assisted process. Also, the higher photosensitivity values for curve B compared with the values for curve C indicates that dressed photons are readily generated inside the Si-PD compared with the case of curve C, as a result of implantation of a high concentration of B.

Because Joule-heat annealing was performed while radiating 1.32  $\mu\text{m}$ -wavelength light for fabricating the Si-PD (see Sect. 3), when light having the same wavelength (1.32  $\mu\text{m}$ ) is incident on the device, it is expected that the photosensitivity will be selectively increased. This wavelength-selective photosensitivity increase has already been observed in the case of photovoltaic devices that we

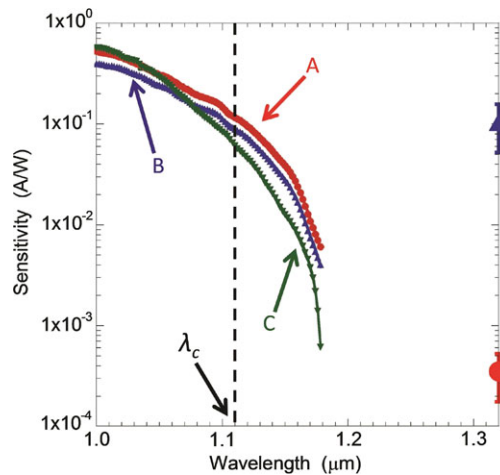


**Fig. 1** Wavelength dependency of photosensitivity. Curve A: device fabricated by phonon-assisted annealing. Curve B: device fabricated without annealing. Curve C: commercially available photodiode (S3590, Hamamatsu Photonics). The red circles and blue triangles show the photosensitivity to incident light (wavelength 1.32  $\mu\text{m}$ ) for forward current densities of 60  $\text{mA}/\text{cm}^2$  and 9  $\text{A}/\text{cm}^2$ , respectively

developed using the phonon-assisted process [17]. Therefore, photosensitivity for incident light with a wavelength of 1.32  $\mu\text{m}$  in particular is discussed in the following. We made a constant forward current flow in the device and evaluated the photosensitivity for incident light with a wavelength of 1.32  $\mu\text{m}$ . Photoelectric conversion in this case involved not only the two-step excitation described by processes (1) and (2) in Sect. 2, but also processes (1') and (2'), but the contribution of the latter was sufficiently large. A semiconductor laser was used as the light source, and the output beam was made incident on the Si-PD after being intensity-modulated with a chopper. We obtained the current variation  $\Delta I = V/R$  from the ratio of the voltage variation  $V$  produced at that time and the resistance  $R$  of the Si-PD, and we divided this by the incident light power  $P$  to obtain the photosensitivity  $\Delta I/P$ . The results are indicated by the red circles and the blue triangles in Fig. 1. These are the measured values for cases where the forward current densities of the fabricated Si-PD were 60  $\text{mA}/\text{cm}^2$  and 9  $\text{A}/\text{cm}^2$ , respectively. The photosensitivity for the current density of 9  $\text{A}/\text{cm}^2$  was 0.10  $\text{A}/\text{W}$ . This is as much as two times higher than the case using mid-bandgap absorption [5–7] described in Sect. 1, demonstrating that we achieved our objective of increasing the photosensitivity. This value is about 300 times higher than the 60  $\text{mA}/\text{cm}^2$  case, and shows the same large values as curve C at a wavelength of 1.09  $\mu\text{m}$ . This photosensitivity is sufficiently high for use in long-distance optical fiber communication systems [22]. The increase in photosensitivity with increasing forward current at a wavelength of 1.32  $\mu\text{m}$  is due to the higher stimulated emission gain as well as the higher number of recombining electrons.

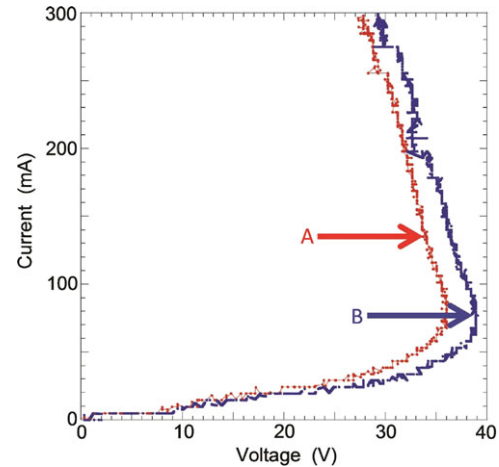


**Fig. 2** Voltage–current characteristics. Curves A and B are measurement results obtained with and without light irradiation

#### 4.2 Voltage–current characteristics and optical amplification characteristics

First, we measured the voltage–current characteristics for cases where the Si-PD was irradiated and not irradiated with 1.32  $\mu\text{m}$ -wavelength, 120 mW-power laser light. The measurement results are shown by curves A and B in Fig. 2. Both curves show negative-resistance characteristics at forward currents of 80 mA and higher, similarly to the case of a Si-LED (see Fig. 4 in Ref. [14]). Also, curve A is shifted toward lower voltages compared with curve B. This shift was particularly remarkable when the forward current was 30 mA and higher. The reason for this is that the electron number density in the conduction band is reduced because a population inversion occurs around a forward current of 30 mA and electrons are consumed for stimulated emission, and as a result, the voltage required for injecting the same number of electrons is decreased. On the other hand, when the forward current is increased further, the amount of shift is reduced. This is because the probability of stimulated emission recombination driven by spontaneous emission is increased as the forward current increases, and as a result, the voltage drop due to stimulated emission recombination caused by incident light becomes relatively small.

Next, we measured the relationship between the incident light power  $P$  and the current variation  $\Delta I$ . For this measurement, we used forward current densities of 60  $\text{mA}/\text{cm}^2$  and 9  $\text{A}/\text{cm}^2$ , and we varied the incident light power by using neutral density filters. In a conventional Si-PD, only absorption of light is used for photoelectric conversion. In our Si-PD, however, because stimulated emission is also used, the current variation  $\Delta I$  depends on the number of electron–hole pairs that recombine due to stimulated emission and is given by  $\Delta I = (eP/h\nu)(G - 1)$ . Here,  $e$  is the electron



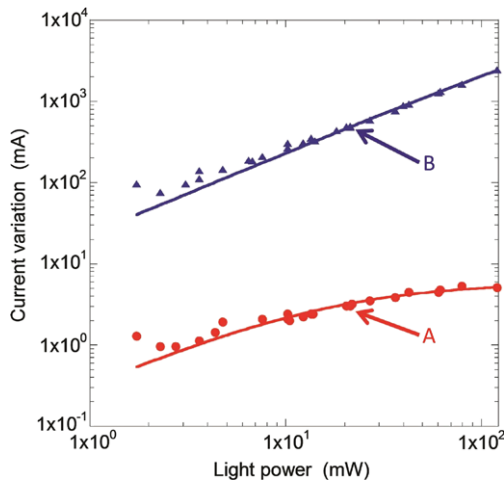


**Fig. 3** Relationship between incident light power (wavelength 1.32  $\mu\text{m}$ ) and current variation. Curves A and B are for forward current densities of 60  $\text{mA}/\text{cm}^2$  and 9  $\text{A}/\text{cm}^2$ , respectively

charge,  $h\nu$  is the photon energy, and  $G$  is the stimulated emission gain.

The relationship between the incident light power at a wavelength of 1.32  $\mu\text{m}$  and the current variation  $\Delta I$  is shown in Fig. 3. Similarly to Fig. 1, the red circles and blue triangles show the measurement results for forward current densities of 60  $\text{mA}/\text{cm}^2$  and 9  $\text{A}/\text{cm}^2$ , respectively. For the forward current density of 60  $\text{mA}/\text{cm}^2$ ,  $\Delta I$  saturated as the incident light power increased; whereas for the forward current density of 9  $\text{A}/\text{cm}^2$ ,  $\Delta I$  did not saturate but continued to increase linearly. The curves A and B show calculation results fitted to the experimental results using the above relationship  $\Delta I = (eP/h\nu) \times (G - 1)$ . The stimulated emission gain  $G$  depends on the incident light power as  $\exp[g/(1 + P/P_s)]$  [23], where  $g$  is the small-signal gain coefficient, and  $P_s$  is the saturation power. For the fitted results, these values were  $g = 3.2 \times 10^{-4}$  and  $P_s = 17$  mW in the case of curve A, and  $g = 2.2 \times 10^{-2}$  and  $P_s = 7.1 \times 10^2$  mW in the case of curve B. The increases in  $g$  and  $P_s$  as the forward current increased were due to the increasing number of electrons recombining. The experimental values and calculated values showed good agreement in Fig. 3, confirming that the remarkable increase in photosensitivity shown by the red circles and blue triangles in Fig. 1 was due to optical amplification as a result of stimulated emission.

#### 4.3 Photosensitivity characteristics with reverse bias

In Sects. 4.1 and 4.2 above, it was shown that the remarkable increase in photosensitivity when a forward current was applied is due to optical amplification based on stimulated emission. In this subsection, in order to verify this,

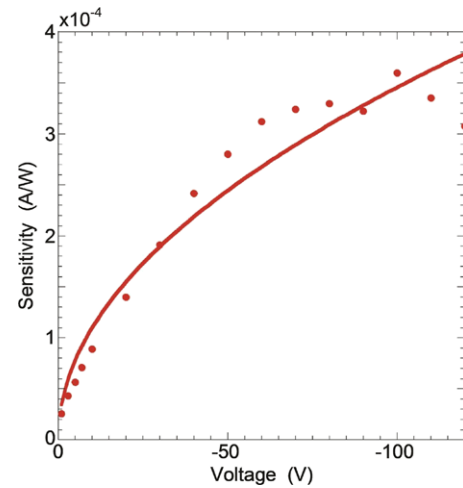


**Fig. 4** Relationship between reverse-bias voltage and photosensitivity. The wavelength of the incident light was 1.32  $\mu\text{m}$

we measured the photosensitivity when a reverse bias voltage  $V_r$  was applied, while keeping the incident light power fixed. The photoelectric conversion in this case is based on the two-step excitation described by processes (1) and (2) in Sect. 2. For these measurements, we set the stabilized power supply to a constant-voltage mode and measured the voltage variation across both ends of a 1  $\text{k}\Omega$  load resistor. The red circles in Fig. 4 are the measurement results of the relationship between the reverse bias voltage and the photosensitivity. The maximum photosensitivity was about  $3 \times 10^{-4}$  A/W, which is about 1/300 of the value (0.10 A/W) indicated by the blue triangles in Fig. 1 (a forward current density of 9  $\text{A}/\text{cm}^2$ ). When  $V_r = 0$ , the photosensitivity was too low to be measured. When the reverse bias voltage was low, for example,  $V_r = -1$  V, the photosensitivity was about  $2.5 \times 10^{-5}$  A/W, and therefore, the value of 0.10 A/W above shows that the photosensitivity at  $V_r = 0$  was amplified by a factor of at least 4000.

This figure shows that the photosensitivity increases as the reverse bias voltage increased, and then saturated. Electron-hole pairs created by light absorption are extracted from the depletion layer, generating photocurrent, and the photocurrent is proportional to the width  $w$  of the depletion layer; therefore, we used the expression  $w = A\sqrt{-V_r}$  [24] representing the relationship between the width  $w$  and the reverse bias voltage  $V_r$ , and the curve in this figure shows the calculation results fitted to the measured values. Because the photosensitivity saturates as the reverse bias voltage increases, no electron avalanche effect [25] occurs. This means that there is no contribution from an avalanche effect in the remarkable increase in photosensitivity observed when a forward current was applied (see Sects. 4.1 and 4.2). Therefore, it was confirmed that this remarkable increase in photosensitivity was due to optical amplification based on stimulated emission.

## 5 Conclusion

We fabricated a new photodetector by subjecting a Si crystal having p–n homojunction to a phonon-assisted annealing process. For incident light with a wavelength of 1.16  $\mu\text{m}$  and higher, this device showed a photosensitivity about three times higher than a Si-PIN photodiode used as a reference. The photosensitivity for 1.32  $\mu\text{m}$ -wavelength incident light was increased by applying a forward current, and we obtained a photosensitivity of 0.10 A/W for a forward current density of 9 A/cm<sup>2</sup>. This value is at least 4000 times greater than the zero-bias photosensitivity, and the remarkable increase was due to the manifestation of optical amplification caused by the forward current injection. For a forward current density of 9 A/cm<sup>2</sup>, the small-signal gain coefficient for optical amplification was  $2.2 \times 10^{-2}$ , and the saturation power was  $7.1 \times 10^2$  mW. There was no contribution from an electron avalanche effect in this behavior. In a future paper, we plan to report details of other characteristics, such as the photosensitivity for incident light in the infrared region at wavelengths other than 1.32  $\mu\text{m}$ , the signal-to-noise ratio, and the frequency response band.

**Open Access** This article is distributed under the terms of the Creative Commons Attribution License which permits any use, distribution, and reproduction in any medium, provided the original author(s) and the source are credited.

## References

1. M. Levinshtein, S. Rumyantsev, M. Shur, *Handbook Series on Semiconductor Parameters*, vol. 1 (World Scientific, Singapore, 1996)
2. A. Loudon, P.A. Hiskett, G.S. Buller, *Opt. Lett.* **27**, 219 (2002)
3. C. Cremer, N. Emeis, M. Schier, G. Heise, G. Ebbinghaus, L. Stoll, *IEEE Photonics Technol. Lett.* **4**, 108 (1992)
4. A.F. Phillips, S.J. Sweeney, A.R. Adams, P.J.A. Thijs, *IEEE J. Sel. Top. Quantum Electron.* **5**, 401 (1999)
5. J.E. Carey, C.H. Crouch, M. Shen, E. Mazur, *Opt. Lett.* **30**, 1773 (2005)
6. M.W. Geis, S.J. Spector, M.E. Grein, R.T. Schuelein, J.U. Yoon, D.M. Lennon, C.M. Wynn, S.T. Palmacci, F. Gan, F.X. Kärtner, T.M. Lyszczarz, *Opt. Express* **15**, 16886 (2007)
7. M.W. Geis, S.J. Spector, M.E. Grein, R.T. Schuelein, J.U. Yoon, D.M. Lennon, F. Gan, F.X. Kärtner, T.M. Lyszczarz, *IEEE Photonics Technol. Lett.* **19**, 152 (2007)
8. T. Baehr-Jones, M. Hochberg, A. Scherer, *Opt. Express* **16**, 1659 (2008)
9. H. Chen, X. Luo, A.W. Poon, *Appl. Phys. Lett.* **95**, 171111 (2009)
10. M. Lee, C. Chu, Y. Wang, *Opt. Lett.* **26**, 160 (2001)
11. M. Cassalino, L. Sirlito, L. Moretti, M. Gioffrè, G. Coppola, *Appl. Phys. Lett.* **92**, 251104 (2008)
12. T. Tanabe, K. Nishiguchi, E. Kuramochi, M. Notomi, *Appl. Phys. Lett.* **96**, 101103 (2010)
13. B. Shi, X. Liu, Z. Chen, G. Jia, K. Cao, Y. Zhang, S. Wang, C. Ren, J. Zhao, *Appl. Phys. B* **93**, 873 (2008)
14. T. Kawazoe, M.A. Mueed, M. Ohtsu, *Appl. Phys. B* **104**, 747 (2011)
15. T. Kawazoe, M. Ohtsu, K. Akahane, N. Yamamoto, *Appl. Phys. B* (2012, in press)
16. T. Kawazoe, K. Kobayashi, S. Takubo, M. Ohtsu, *J. Chem. Phys.* **122**, 024715 (2005)
17. S. Yukutake, T. Kawazoe, T. Yatsui, W. Nomura, K. Kitamura, M. Ohtsu, *Appl. Phys. B, Lasers Opt.* **99**, 415 (2010)
18. T. Kawazoe, M. Ohtsu, Y. Inao, R. Kuroda, *J. Nanophotonics* **1**, 011595 (2007)
19. T. Yatsui, K. Hirata, W. Nomura, Y. Tabata, M. Ohtsu, *Appl. Phys. B* **93**, 55 (2008)
20. T. Kawazoe, H. Fujiwara, K. Kobayashi, M. Ohtsu, *IEEE J. Sel. Top. Quantum Electron.* **15**, 1380 (2009)
21. M.G.A. Bernard, G. Duraffourg, *Phys. Status Solidi* **1**, 699 (1961)
22. J.D. Schaub, *J. Lightwave Technol.* **19**, 272 (2001)
23. T. Saitoh, T. Mukai, *IEEE J. Quantum Electron.* **23**, 1010 (1987)
24. N.W. Ashcroft, N.D. Mermin, *Solid State Physics* (Brooks Cole, Singapore, 1976)
25. R.J. McIntyre, *IEEE Trans. Electron Devices* **13**, 164 (1966)